scientific reports

Check for updates

OPEN

Fenugreek seeds as a natural source of L-arginine-encapsulated lipid nanoparticles against diabetes

Urooj Ali[1,2], Syeda Izma Makhdoom[3], Muhammad Uzair Javed[1], Rafia Ali Khan[4], Muhammad Naveed[3], Bilal Haider Abbasi[1,5]✉, Tariq Aziz[6]✉, Fatma Alshehri[7], Fahad Al-Asmari[8], Fakhria A. Al-Joufi[9] & Maher S. Alwethaynani[10]

Diabetes, affecting over 10.5% of the global population, leads to severe health complications and economic burdens, highlighting the urgent need for effective therapeutic approaches. Current treatments are often insufficient, prompting the exploration of novel therapeutic agents and delivery mechanisms. This study addresses this gap by investigating the roles of L-arginine (identified as a target drug candidate through network pharmacology) in diabetes management, while also evaluating lipid nanocarriers synthesized from fenugreek seed oil for improved drug delivery. Our docking analyses revealed L-arginine's strong interactions with diabetes-target genes (CYP1A2, CYP2C19, and NFKB), with multiple hydrogen bonds and binding energies ranging from – 7.2 to – 8.9 kcal/mol. Encapsulated L-arginine lipid nanoparticles were characterized using UV-Visible spectroscopy, showing absorbance peaks at 415 nm for simple nanoparticles and 521 nm for L-arginine-loaded nanoparticles. Scanning electron microscopy confirmed an average nanoparticle size of 100.2 nm, and zeta potential analysis indicated a neutral surface charge (– 9.37 mV). Antioxidative activity showed 84.44% inhibition with an IC50 value of 40.5 µg/mL The nanoparticles inhibited albumin denaturation by 81.10% and alpha-amylase by 89.30%, surpassing metformin (78.43% at 1000 µg/mL). Hemolysis percentage was minimal at 10.54%. These findings demonstrate the potential of L-arginine as an anti-diabetic agent and highlight the efficacy of lipid nanocarriers as innovative drug delivery systems, providing a foundation for advancing therapeutic interventions against diabetes.

Keywords Diabetes, *Trigonella foenum-graecum*, L-arginine, Lipid nanoparticles, Network pharmacology

Diabetes is a complex metabolic disorder that substantially impacts the overall well-being of individuals worldwide including mental health[1]. The condition is distinguished by chronic hyperglycemia, which arises from impairments in either insulin secretion, insulin action, or both. The rising incidence of diabetes worldwide seriously affects public health and healthcare delivery worldwide. About 10.5% of the adult population (20–79 years) globally has diabetes, and roughly half of them is ignorant of their illness, according to the International Diabetes Federation[2]. Since 1980, the percentage of adults with diabetes has almost doubled, from 4.7 to 8.5%, till 2021. Globally, diabetes affects approximately 10.5% of the adult population, with projections indicating a rise to 643 million by 2030 and 783 million by 2045[3]. This rising prevalence emphasizes on the urgent need for innovative therapeutic strategies. Despite a wide range of antidiabetic medications, such as flavonoids, biguanides, sulfonylureas, selenoproteins, and GLP-1 receptor agonists, current treatments often fail to address critical issues, including drug stability, bioavailability, and long-term efficacy[4,5]. These limitations necessitate alternative approaches that enhance drug delivery and target glucose metabolism more effectively. Traditional

[1]Department of Biotechnology, Quaid-I-Azam University, Islamabad 45320, Pakistan. [2]Faculty of Life and Environmental Sciences, School of Science, The University of Sydney, Camperdown, Sydney, NSW 2050, Australia. [3]Department of Biotechnology, Faculty of Science and Technology, University of Central Punjab, Lahore 54590, Pakistan. [4]Faculty of Pharmaceutical Sciences, University of Central Punjab, Lahore 54590, Pakistan. [5]EA2106 Biomolécules et Biotechnologies Végétales, Université de Tours, Tours 37000, France. [6]Laboratory of Animal Health Food Hygiene and Quality, University of Ioannina, Arta, Greece. [7]Department of Biology, College of Sciences, Princess Nourah bint Abdulrahman University, P.O. Box 84428, Riyadh 11671, Saudi Arabia. [8]Department of Food and Nutrition Sciences, College of Agricultural and Food Sciences, King Faisal University, Al Ahsa 31982, Saudi Arabia. [9]Department of Pharmacology, College of Pharmacy, Jouf University, Aljouf 72341, Saudi Arabia. [10]Department of Clinical Laboratory Sciences, College of Applied Medical Sciences, Shaqra University, Alquwayiyah, Riyadh, Saudi Arabia. ✉email: bhabbasi@qau.edu.pk; iwockd@gmail.com

medical practices worldwide have long recognized the usefulness of plant-based medicines, valued for their bioactive phytochemicals such as polyphenols, flavonoids, alkaloids, and terpenoids. These compounds exhibit antioxidant, anti-inflammatory, and anti-diabetic properties[6,7].

Fenugreek (*Trigonella foenum-graecum*), a plant widely cultivated across Asia, Europe, and North Africa, has demonstrated notable hypoglycemic effects[8]. Its phytochemicals, including diosgenin, 4-hydroxyisoleucine, and trigonelline, have been shown to improve insulin sensitivity and reduce oxidative stress, making it a promising candidate for diabetes management[9]. Animal studies have further substantiated the anti-diabetic potential of Fenugreek, indicating that fenugreek extract can decrease blood glucose levels in animal models with diabetes[10,11]. L-arginine, a semi-essential amino acid, has attracted considerable interest in diabetes research due to its potential therapeutic properties against diabetes. It is a precursor for synthesizing nitric oxide (NO), a potent vasodilator pivotal in regulating blood flow and vascular function[12]. Furthermore, previous studies have demonstrated that L-arginine can mitigate the detrimental effects of glucotoxicity and lipotoxicity on pancreatic beta-cell dysfunction and apoptosis[13,14].

However, its therapeutic potential is limited by poor bioavailability and rapid clearance when administered alone[15]. Encapsulation in lipid nanocarriers—a strategy shown to improve drug stability, targeted delivery, and controlled release—offers a potential solution to these challenges[16]. While lipid nanocarriers have been widely explored for the delivery of various therapeutic agents[17], their application for encapsulating L-arginine remains underexplored. This study provides a novel approach by using lipid nanocarriers not only to overcome the limitations of L-arginine's bioavailability but also to enhance its therapeutic efficacy in glucose regulation. Taking Fenugreek seed oil as the lipid source, this research introduces a dual-action delivery system that integrates the proven hypoglycemic properties of fenugreek phytochemicals with the antioxidative and beta-cell protective effects of L-arginine. Instead of focusing on a direct cure, our objective was to explore how L-arginine-loaded lipid nanocarriers can improve drug delivery and bioavailability.

This research integrates network pharmacology to elucidate the molecular pathways involved in the therapeutic action of L-arginine and fenugreek. Combined with phyto-informatics and comparative in vitro trials against metformin, this study aims to establish a novel foundation for future diabetes treatments. By addressing gaps in current therapies, this work also emphasizes the potential of lipid nanocarriers for delivering innovative and effective antidiabetic interventions.

Materials and methods
Plant and seed selection
The research conducted by Tariq et al.[18] regarding the utilization of herbal medicines for diabetes treatment in the Southern regions of Pakistan, along with its associated pharmacological evidence, served as a pivotal reference for this study. From the pool of identified plants in the study[18], Fenugreek emerged as the primary focus of this study. The rationale behind this selection was multi-faceted. A thorough review of scholarly sources[11,19,20] provided substantive evidence suggesting that fenugreek seeds have significant therapeutic attributes. Two hundred fifty grams of fenugreek seeds were procured from a reputable local source, namely the Kashmiri Dawa Khana establishment in Wazirabad, Punjab, Pakistan.

Network pharmacology for active compound identification
The Collective Molecular Activities of Useful Plants (CMAUP) database[21], accessible at https://bidd.group/CMAUP/, was used to assess fenugreek's therapeutic potential systematically. Compounds extracted from the CMAUP database formed the foundational basis for exploring potential anti-diabetic attributes. Concurrently, identifying biological targets associated with these active compounds was also achieved through data from the CMAUP database. The UniProt database[22] was used to ensure data standardization and coherence (accessible at https://www.uniprot.org/) by converting target protein names into standardized target gene names.

Identification of T2DM gene targets and collective targets
T2DM-associated targets were searched within the GeneCards platform[23] (accessible at https://www.genecards.org/), employing "type 2 diabetes mellitus" and "T2DM" as primary keywords, with a focus on the *Homo sapiens* species. Subsequently, these targets, identified from the identified fenugreek compounds and those linked to type 2 diabetes mellitus, were merged with the removal of duplicate entries. The pinpointing of shared targets among the fenugreek compounds and T2DM targets was achieved VENNY 2.1[24] (accessible at https://bioinfogp.cnb.csic.es/tools/venny/).

Network visualization of target genes and active compounds
Cytoscape 3.9.1[25] (accessible at http://www.cytoscape.org/) served as a dynamic visual representation tool, elucidating the interplay between the bioactive compounds present in Fenugreek and the T2DM-associated targets. Multi-colored cells displayed the common targets between fenugreek compounds and T2DM.

Protein-protein network analysis
The overlapping targets, resulting from the earlier analysis, were subjected to interaction assessment using STRING 11.0 (Search Tool for the Retrieval of Interacting Genes/Proteins), accessible at https://string-db.org/. We utilized the "multiple protein" module within STRING to ensure a focused examination of the protein-protein associations. The gene type was specified as *Homo sapiens* to ensure a relevant context. The generated network visualization distinguished nodes by color and content according to the work of Szklarczyk et al.[26].

Molecular Docking of target proteins and active compounds

Molecular Operating Environment (MOE) software[27] was used to investigate the molecular interactions between the core gene targets and Fenugreek's active compounds. The protein structures (Table 1), acquired from the Protein Data Bank (PDB)[28], accessible at: https://www.rcsb.org/, comprised the three-dimensional (3D) structures essential for the docking study. While three primary diabetes-associated protein targets (CYP1A2, CYP2C19, and NFKB) were selected based on our network pharmacology analysis, this limited scope may not encompass the full breadth of molecular interactions associated with fenugreek's bioactive compounds. Future studies should aim to include additional targets, such as insulin receptors or glucose transporters, to broaden the understanding of their therapeutic potential. Using the Discovery Studio software 2021 client (downloaded from https://discover.3ds.com/discovery-studio-visualizer-download), we purified the protein structures of extraneous elements, notably water molecules, and ligands. The induced fit model was chosen for the docking refinement within the Molecular Operating Environment (MOE). The initial scoring method was chosen as London dG, whereas the final scoring function was chosen as GBVI/WSA dG with 5 docking poses. We used metformin (accessed at: https://pubchem.ncbi.nlm.nih.gov/compound/Metformin, PubChem ID: 4091) as a reference point for comparing the relative binding affinities of the identified fenugreek compounds.

Absorption, distribution, metabolism, excretion, and toxicity (ADMET) analysis

ADMET analysis was performed to evaluate our target compounds' pharmacokinetic properties comprehensively. We utilized two pivotal criteria from the literature[29]: compounds with oral bioavailability (OB) greater than or equal to 30% were considered to possess favorable absorption and metabolism characteristics following oral administration. Compounds with a drug-likeness (DL) score equal to or exceeding 0.18 were deemed chemically suitable for drug development. SwissADME[30] (accessed at: http://www.swissadme.ch/) and ADMET LAB 2.0[31] (https://admetmesh.scbdd.com/) provided a comprehensive understanding of the pharmacokinetic viability of our target compounds.

Seed extract preparation

Twenty grams of Fenugreek seeds were washed thrice with distilled water and subsequently air-dried. The desiccated seeds were then finely powdered utilizing an electric grinder. Methanol was selected as the extraction solvent due to its effectiveness in extracting a broad spectrum of bioactive compounds, including flavonoids, alkaloids, and polyphenols, as supported by literature[8]. A mixture of 100 mL of methanol and 20 g of finely ground fenugreek seeds was prepared in a 250 mL beaker. To optimize extraction efficiency, ultrasonication was conducted at 50 °C for 60 min, a parameter chosen based on its ability to enhance the release of bioactive constituents by disrupting cellular matrices while preserving compound stability. After sonication, the mixture was filtered to remove solid residues, and the filtrate was stored at 4 °C in a laboratory refrigerator for subsequent use in the production of lipid nanoparticles.

Seed oil preparation

Dried and ground fenugreek seeds, weighing 30 g, were used in the oil extraction process using the Soxhlet apparatus. The fenugreek seeds accurately weighed, were introduced into the thimble. A volume of 300 ml of chloromethane, the selected solvent, was added to the round-bottom flask. The solvent level was maintained below the thimble in the fully assembled apparatus. The extraction procedure was allowed to proceed overnight,
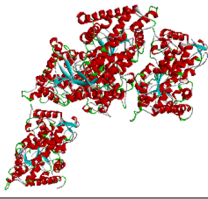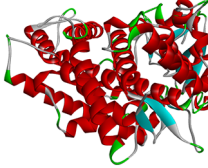
Target protein	PDB ID	Length	Molecular weight	3D structure
CYP2C19	4GQS	477 amino acids	222.19 kDa	
CYP1A2	2HI4	495 amino acids	57.18 kDA	
NFKB-1	1NFK	325 amino acids	79.89 kDa	

Table 1. Core protein targets selected for molecular docking.

at room temperature, approximately for 12 h. A transfer of the extracted oil from the round-bottom flask was performed upon the thorough removal of residual solvent. The oil was then filtered and stored.

Phytochemical screening

We conducted a phytochemical screening on both seed extract and oil extract derived from fenugreek seeds. Wagner's test was performed to ascertain the presence of alkaloids. Separate seed and oil extract samples (2–3 mL) were introduced into individual test tubes. Subsequently, the seed tincture was supplemented with 1 mL of HCl and several drops of Wagner's reagent. Vigorous agitation of the test tube resulted in the appearance of a reddish-brown hue, which served as an indicative marker of the alkaloid presence. The foam test differentiated saponins within the seed and oil extract solution. Equal volumes of seed and oil extract (5 mL) were combined with purified water (5 mL) and subjected to vigorous shaking. A stable foam formation was observed, indicating the presence of saponins.

The ferric chloride test facilitated the detection of phenols within the seed tincture and oil extract. 5 mL of seed and oil extract were introduced into separate test tubes, followed by a few drops of neutral 5% ferric chloride solution. The resulting interaction led to a distinctive blue-green coloration, confirming the presence of phenols. The identification of tannins was accomplished through Braymer's test. It involved the addition of 2 mL of purified water and several drops of ferric chloride solution to 2 mL of seed tincture and oil extract. The appearance of green precipitates within the solutions signified the presence of tannins. To demonstrate the existence of terpenoids within the extracted seed tincture and oil extract, Salkowski's test was conducted. To this end, 2 mL of seed tincture and oil extract were combined with 2 mL of chloroform and 2 mL of concentrated H_2SO_4. The development of a discernible yellow coloration served as an indication of the presence of terpenoids.

Phytochemical quinones were assessed using Bontrager's test. A layer was separated by adding 3 mL of chloroform to 3 mL of seed tincture and oil extract. The subsequent addition of 5% potassium hydroxide to the formed layer resulted in a pronounced red coloration, confirming the presence of quinones. Screening cardiac glycosides within the prepared seed extract and oil extract involved Keller Killian's test. It combined 2 mL of HCl, sodium nitroprusside, and sodium hydroxide with 2 mL of seed extract and oil extract. The emergence of a pink to crimson coloration indicated the presence of cardiac glycosides. The identification of phytochemical glycosides was executed through the glycosides test.

In this process, 2 mL of seed tincture and oil extract were combined with 3 mL of chloroform and 10% alkali solution. The manifestation of a pink coloration confirmed the presence of glycosides. The alkaline reagent test ascertained the presence of flavonoids within the seed tincture and oil extract. A distinct yellow coloration emerged by introducing NaOH to 2 mL of seed extract and oil extract, signifying the presence of flavonoids. The screening for phytochemical phlobatannins was conducted through the precipitate test. Adding a few drops of 2% HCl to 1 mL of seed extract and oil extract resulted in the formation of red precipitates, thereby confirming the presence of phlobatannins within the extracted seed tincture and oil extract.

Evaluation of total flavonoid content

The total flavonoid content was quantified following a methodology stipulated by Singleton et al.[32] using the aluminum chloride colorimetric technique. Quercetin, chosen as a standard reference, was solubilized in methanol to establish a standard curve across a concentration range of 50–250 µg/mL. In a volumetric flask, a solution containing 0.5 mL of both fenugreek seed and oil extracts was combined with 0.1 mL of a 10% w/v aluminum chloride solution, and 0.1 mL of a 0.1 mM potassium acetate solution. Absorbance measurements were ascertained utilizing a UV–Vis spectrophotometer at a wavelength of 715 nm. The quantification of total flavonoid content was achieved by utilizing the quercetin calibration curve (Fig. 1), as the equation y = 0.0042x – 0.1149, demonstrating a commendable coefficient of determination (R^2) value of 0.998. The outcomes were expressed in terms of the extract's quercetin equivalent (QE) per milligram per gram (mg/g).

The computation of the total flavonoid content (TFC) was performed using the formula:

$$Total \ Flavonoid \ content \ (mg/g) = \frac{C \times V}{M}$$
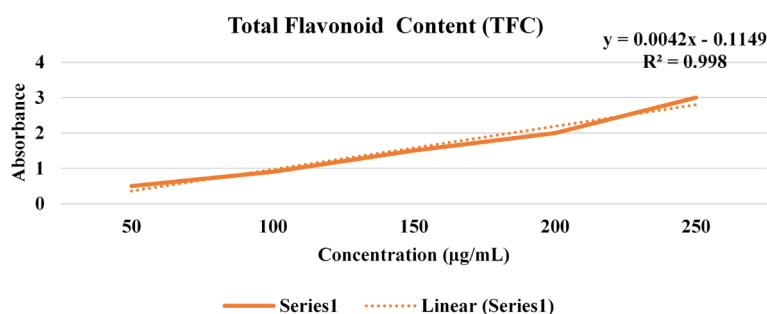
Where:

Fig. 1. TFC content of fenugreek.

C signifies the concentration of the determined fractions derived from the quercetin calibration curve. V indicates the volume of the extract in milliliters (mL). M denotes the weight of the dry fenugreek seed and oil extract in grams (g).

Evaluation of total phenolic content

Singleton et al.[32] further explained the utilization of the Folin–Ciocalteu reagent in quantifying the total phenolic content (TPC). 0.5 mL of fenugreek seed and oil extracts were mixed manually with 2.5 mL of the Folin–Ciocalteu reagent. The resultant mixtures underwent an incubation period of 15 min at 37 °C. Following this, 2 mL of sodium carbonate (Na_2CO_3) solution (7.5% w/v) was added, followed by a volume adjustment to 10 mL with distilled water. A subsequent 30-minute incubation transpired before triplicating spectrophotometric measurements were conducted at a wavelength of 760 nm. A standard curve (Fig. 2) was established using gallic acid as a reference compound. The concentrations of gallic acid ranged from 50 to 250 μg/mL. The quantification of total phenols was expressed as gallic acid equivalents (GAE) in milligrams per gram (mg/g) of dry weight, employing the equation $y = 0.0037x - 0.094$, which yielded an impressive coefficient of determination (R^2) value of 0.999.

The computation of the total phenolic content (TPC) was performed utilizing the formula:

$$Total\ Phenolic\ Content\ (mg/g) = \frac{C \times V}{M}$$

Where:

C signifies the concentration of the determined fractions extrapolated from the gallic acid calibration curve. V represents the volume of the extract in milliliters (mL). M indicates the weight of the dry plant extract in grams (g).

Synthesis of lipid nanoparticles

Lipid nanoparticles were synthesized through the controlled mixing of methanolic seed extract and seed oil derived from Fenugreek seeds, adhering to a fixed 1:1 volumetric ratio. To mitigate the potential influence of light exposure during the reaction, the sequential addition of seed extract and seed oil was administered dropwise while maintaining a consistent stirring rate of 1500 rpm on a magnetic stirrer. The solution was subjected to continuous stirring in darkness at room temperature for 30 min and examined within a UV-Vis spectrophotometer across the defined wavelength range of 450–800 nm.

Encapsulation of L-arginine in lipid nanoparticles

An aqueous solution of L-arginine was prepared through a controlled combination of the lipid nanoparticles and the L-arginine solution, achieved at a volumetric ratio of 2:1 respectively. This mixing was executed through high-speed stirring at 1500 rpm, inducing the formation of a pre-emulsion. The resulting pre-emulsion was introduced drop by drop into an aqueous solution containing a stabilizer while maintaining constant stirring. The nanoparticle solution was centrifuged, operating at a speed of 40,000 rpm for 30 min. The cleaned pellet was then transferred to an evaporating dish and subjected to a drying process of 6–7 h, within a hot air oven set at 80 °C.

Characterization of the synthesized nanoparticles

The validation of the presence of synthesized lipid nanoparticles encapsulating L-arginine was accomplished through the utilization of a UV-visible spectrophotometer, focusing on the surface plasmon resonance band between 200 and 800 nm. This band shows maximum absorption, confirming successful synthesis and surface plasmon vibration activation. The structural characteristics of the acquired nanoparticles were elucidated via Scanning Electron Microscopy (SEM). Samples of the synthesized L-arginine encapsulated lipid nanoparticles, in their dried state, were positioned on double-conductive tape affixed to a designated sample holder. A platinum–gold coating was applied to enhance electrical conductivity. The samples were examined using scanning electron microscopy (SEM) under a voltage of 12.50 kV. Distinctive functional groups intrinsic to the synthesis of L-arginine encapsulated lipid nanoparticles were evaluated through Fourier Transform Infrared Spectroscopy
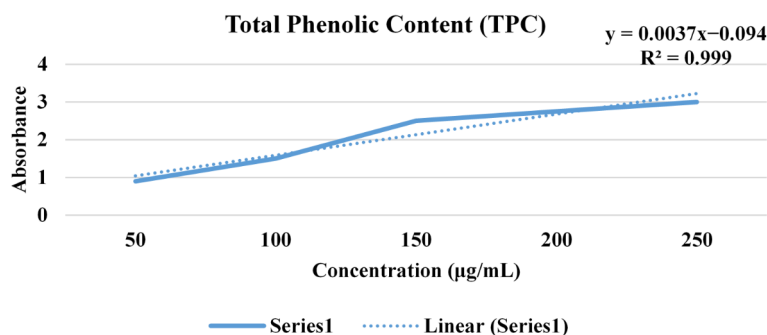

Fig. 2. TPC content of fenugreek.

(FTIR). The solution containing the resultant lipid nanoparticles underwent prior centrifugation at 10,000 rpm for 30 min before acquiring FTIR measurements.

The particle size analysis used a Laser Scattering Particle Size Distribution Analyzer (Model: LA-300, Manufacturer: Horiba, Japan). The analyzer, operating with a 650 nm Laser diode (5 mW) as the light source and a photomultiplier tube as the detector, determined particle size and distribution state. Dimethyl sulfoxide (DMSO) was selected as the solvent due to its compatibility with the sample and its ability to dissolve hydrophobic components effectively. A dilute sample of 10 mL was prepared and sonicated for 20 min to prevent aggregation. The measurements were conducted using a cuvette cell as the container, and each measurement lasted approximately 2 min.

The Zetasizer Nano ZSP (Model: Malvern Zetasizer Nano ZSP, Manufacturer: Malvern Panalytical, Malvern, UK) was used for the measurement of particle size, electrophoretic mobility of proteins, zeta potential of nanoparticles and surfaces, and optionally, micro rheology of protein and polymer solutions. The choice of DMSO as the solvent ensured consistent dispersion of nanoparticles, and the sonication process (20 min) was implemented to minimize aggregation and improve measurement accuracy. A dilute sample of 10 mL was prepared for analysis. The nature of the biosynthesized L-arginine-encapsulated lipid nanoparticles was investigated through X-ray diffraction (XRD) analysis. A powdered sample of the nanoparticles was used, and XRD measurements were conducted in scanning mode using a current of 30 mA and a voltage of 40 kV. Cu/Kα radiation was utilized, and the diffraction pattern was recorded over a 2θ angle range of 20° to 70°. To determine the average crystalline size of the lipid nanoparticles, the Debye–Scherrer equation was applied to determine the average crystalline size of the lipid nanoparticles, chosen for its reliability in calculating nanoscale crystallite sizes.

$$D = \frac{k\lambda}{\beta \cos\theta}$$

In this equation:

D represents the average crystalline size of the nanoparticles. k is the shape factor with a value of 0.94. λ stands for the X-ray wavelength (λ = 1.5418 Å) for Cu/Kα radiation. β corresponds to the full width at half maximum (FWHM) of the diffraction peak in radians. θ represents Bragg's angle, which is the angle at which constructive interference occurs for a specific lattice plane.

Anti-oxidant assay

Using a 2,2-diphenyl-1-picrylhydrazyl radical (DPPH)-based assay, based on the works of Naveed et al.[33], Ghosh et al.[34]; Ghosh et al.[35], we investigated the capacity of methanolic seed extract, seed oil, and synthetically encapsulated L-arginine lipid nanoparticles to scavenge free radicals. Initially, 3.94 mg of DPPH was dissolved in 100 mL of methanol, yielding a 0.1 mM solution stored in darkness at room temperature to prevent light exposure. The concentration of DPPH was chosen based on its efficacy in yielding reproducible and sensitive measurements of free radical scavenging activity, as established in previous[33–35]. A 0.1 mM solution is widely used as it provides optimal absorbance at 517 nm, ensuring accurate detection of scavenging activity. Subsequently, individual combinations of the prepared methanolic seed extract, seed oil, and encapsulated lipid nanoparticles were each treated with 0.1 mL of 0.1 mm DPPH solution. After a 30-minute incubation period, the absorbance at 517 nm was measured against the positive control, DPPH. The free radical scavenging analysis was conducted in triplicate, and the percentage of DPPH inhibition was calculated using the formula:

$$\% \ DPPH \ Inhibition = \frac{A_o - A_s}{A_o} \times 100$$

Here, A_o denotes the absorbance of the control, and A_s represents the absorbance of the test sample, measured through UV-visible spectroscopy at 517 nm.

Anti-inflammatory activity

Following the protocol of Naveed et al.[33], the anti-inflammatory effects of L-arginine encapsulated lipid nanoparticles were assessed through the protein denaturation method, The procedure involved the combination of the following constituents: 2.8 mL of phosphate-buffered saline solution (pH 6.4), 0.2 mL of hen's egg white, and varying concentrations of 150, 250, 350, 450, and 550 g/mL of the respective methanolic seed extract, seed oil, and synthetic L-arginine encapsulated lipid nanoparticles. These concentrations were chosen to ensure a comprehensive dose-response analysis, capturing both threshold and saturation effects. After an incubation period of 20 min at 37 °C, the mixture was further subjected to a temperature of 70 °C for 5 min to induce protein denaturation. Post-cooling, the turbidity was quantified at 660 nm using a UV-Vis spectrophotometer, as this wavelength is optimal for detecting protein precipitation. An anti-inflammatory reference (acetylsalicylic acid) was used for comparative purposes at concentrations mirroring the experimental samples (150, 250, 350, 450, and 550 g/mL). The anti-inflammatory analysis was executed in triplicate, and the protein inhibition percentage was calculated utilizing the formula:

$$\% \ Inhibition \ of \ Protein \ Denaturation = 1 - \frac{A_s}{A_o} \times 100$$

A_o signifies the absorbance of the control, and A_s represents the absorbance of the test sample, both measured via UV-visible spectroscopy at 660 nm.

Anti-diabetic assay

The antidiabetic activity was assessed utilizing the alpha-amylase test[33]. In each test tube (metformin as control, methanolic seed extract, seed oil, and synthetic L-arginine encapsulated lipid nanoparticles at concentrations 200, 400, 600, 800, and 1000 µL, which allowed for both minimal and maximal detection of inhibitory effects), 10 µL of the alpha-amylase solution (1 unit of alpha amylase) was introduced, followed by thorough manual mixing and subsequent incubation at 30 °C for 10 min to optimize enzyme-substrate interaction. After incubation, a 50 µL aliquot of a 1% starch solution was added, and the mixture was incubated for an additional 1 h at 37 °C. Each test tube was then supplemented with 50 µL of a 1% iodine solution, followed by further incubation for 30 min at 37 °C. The absorbance measurement was conducted utilizing an ELISA reader set to a wavelength of 630 nm, chosen for its ability to detect starch-iodine complexes. This method facilitated the evaluation of the antidiabetic potential of the tested samples, using the following equation.

$$\% \ Inhibition = \frac{Abs_{control} - Abs_{sample}}{Abs_{control}} \times 100$$

Hemolytic activity

A 3 mL aliquot of human blood (ethical permission was taken from the ethical institutional review board, Office of Research Innovation and Commercialization, University of Central Punjab, where this assay was conducted) was drawn and introduced into an EDTA vial, followed by inversion for thorough mixing. The sample was then carefully transferred to a 15 mL tube and subjected to centrifugation at an acceleration of 850 g for approximately 5 min, as this speed is sufficient for effective separation of red blood cells without causing mechanical lysis[36,37]. Pellet was washed with phosphate-buffered saline (PBS) at approximately 4 °C, while the supernatant was subsequently discarded. A suspension was then prepared by adding chilled PBS to achieve a final volume of 20 mL within a Falcon tube. Varying volumes of 150, 250, 350, 450, and 550 µL of the methanolic seed extract, seed oil, and synthetic L-arginine encapsulated lipid nanoparticles were combined with 0.2 mL of the blood suspension within microcentrifuge tubes. These concentrations were chosen to evaluate hemolytic activity across a broad dose range. After a 30-minute incubation at 37 °C, the absorbance was measured at 630 nm using an ELISA reader. This wavelength is optimal for detecting hemoglobin release into the supernatant, a direct indicator of hemolysis. This measurement was conducted after a 15-minute centrifugation at 16,000 rpm, followed by collecting and mixing 100 µL of the resulting supernatant. For comparative assessment, 0.1% Triton X-100 was utilized as the positive control, due to its known ability to induce complete hemolysis, while PBS served as the reference standard in these experiments. The hemolysis percentage was calculated using the following formula:

$$\% \ Hemolysis = \frac{Abs_{sample} - Abs_{negative \ control}}{Abs_{positive \ control}} \times 100$$

Statistical analysis

All assays were performed in triplicate to ensure accuracy and reproducibility. Statistical analysis was conducted using SPSS software version 2020. Results were considered statistically significant by performing One-Way ANOVA at a significance level of $p < 0.05$. Post-hoc comparisons were conducted using Fisher's Least Significant Difference (LSD) test to identify significant differences between groups.

Results

Network pharmacology analysis

The CMAUP database identified 172 unique compounds inherent to fenugreek. Among these, L-arginine and Daidzein emerged as key target compounds for type 2 diabetes mellitus (T2DM). Figure 3A categorizes the diseases targeted by fenugreek, showcasing its diverse therapeutic applications, with T2DM highlighted. Figure 3B illustrates the compound-target activity chart, where deeper red shades represent higher therapeutic potential, diminishing as the red lightens. L-arginine's activity profile is highlighted in the green box, Daidzein's in the yellow box, and common gene targets in purple boxes.

Identification of gene/protein targets

From GeneCards, 14,327 T2DM-related gene/protein targets were identified. The CMAUP database further revealed 10 targets for L-arginine and 55 targets for Daidzein. Aligning these 65 compound-specific targets with the T2DM targets identified three shared targets, visualized in a Venn diagram (Fig. 4).

Network visualization of common genes

Using Cytoscape, the shared gene targets for L-arginine, Daidzein, and T2DM were organized into a network (Fig. 5). Gene targets specific to Daidzein are shown in pink, those specific to L-arginine in green, and the shared targets in yellow.

Protein-protein network analysis

The STRING database provided detailed interaction networks for the protein targets. Figure 6A displays the network of proteins targeted by L-arginine, Fig. 6B shows the network for Daidzein, and Fig. 6C highlights the common proteins shared by both compounds in the context of T2DM.
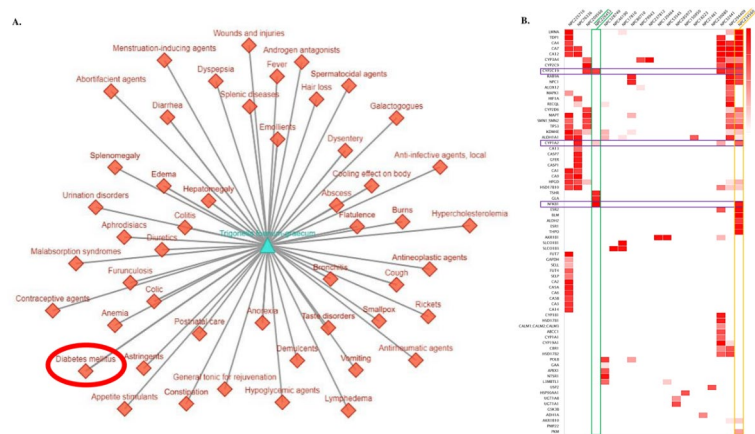
Fig. 3. Therapeutic activity of fenugreek. (A) Diseases targeted by fenugreek; our target disease is highlighted in the red circle; (B) Activity profiles of fenugreek's active compounds. The green box highlights L-arginine's activity profile, the yellow box highlights Daidzein's activity profile and the purple boxes highlight the common gene targets of these compounds.
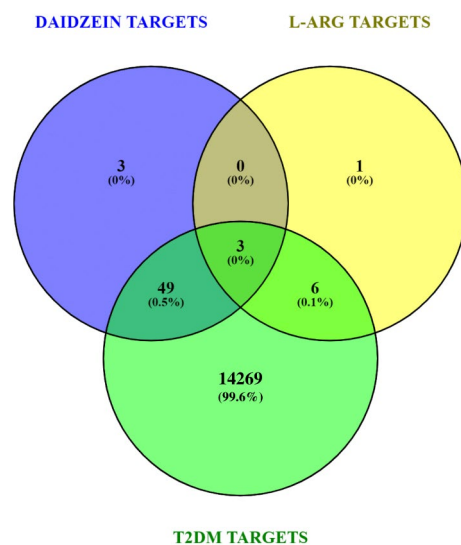

Fig. 4. Venn diagram showcasing the common gene/protein targets of T2DM and the active compounds.

Molecular docking analysis

L-arginine (PubChem ID: 6322), Daidzein (PubChem ID: 5281708), and Metformin (PubChem ID: 4091) were docked against the common protein targets (Table 1). The resultant docking energy scores (Table 2) quantified the molecular interactions, outlining the relative affinities of these compounds toward the identified protein targets. The docking analyses utilized the London dG scoring function for initial scoring, which estimates the binding free energy of the ligand-protein complex in its docked state. For refinement, the GBVI/WSA dG scoring function was used, which provides a more accurate estimation of binding free energy by considering solvation effects and the protein-ligand binding environment. Figure 7 provides the molecular interactions with CYP1A2. Daidzein's arene interactions in the third and fourth pose, juxtaposed against Metformin's solitary sidechain hydrogen bonding in the second pose. L-arginine emerged as the best, with the strongest sidechain and backbone hydrogen interactions, exhibited in four out of five docking poses. Daidzein and Metformin partake in singular sidechain hydrogen bonding instances with CYP2C19 Fig. 8. L-arginine engaged in multiple sidechain and backbone hydrogen bonding interactions in two out of five poses. Similarly, if we look at NFKB-1 interactions (Fig. 9), Daiadzein shows no interaction, Metformin's intermittent interactions in three poses and the predominance of L-arginine is clear with multiple hydrogen bondings in four out of five poses. L-arginine emerged as a potent lead compound, exhibiting more interaction and binding affinity than Daidzein and Metformin.
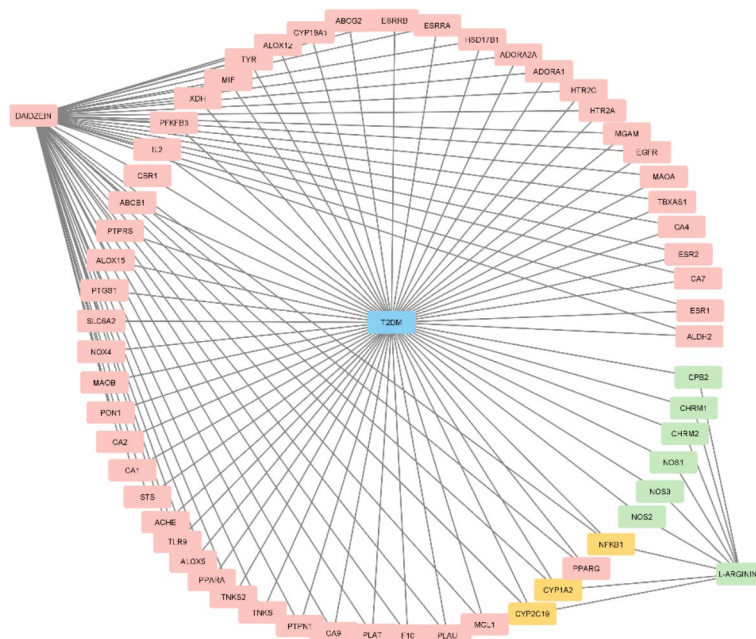
Fig. 5. Cytoscape network of gene/protein targets of the active compounds. Genes in pink are targeted by Daidzein, genes in green are targeted by L-arginine, while those in yellow are targeted by both.
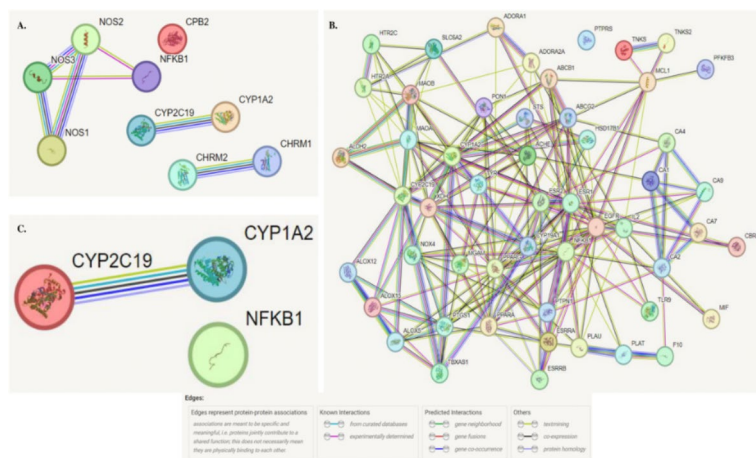

Fig. 6. STRING networks of the gene targets. (A) Network of L-arginine targets; (B) Network of Daidzein targets; (C) Network of the three common gene targets.

ADMET profiles of the target compounds

According to ADMET profiles, Daidzein is acceptable in 6 out of 8 medicinal chemistry analyses, bearing a sole alert pertinent to thiol-reactive compounds. In stark contrast, L-arginine renders acceptability in 5 out of 8 analyses, notably without alarms. The absorption analysis highlights favorable prospects for Daidzein and L-arginine, as evidenced by satisfactory outcomes in 5 out of 7 evaluations. Regarding distribution, L-arginine forges ahead, securing 3 out of 4 satisfactory results compared to Daidzein's attainment of 2 out of 4. Moreover, L-arginine's non-blood-brain-barrier permeability, noticeable through the BOILED-EGG model (Fig. 10E), substantiates its therapeutic potential against T2DM.

Both compounds evade cautionary signals in toxicophore analyses, with L-arginine evincing non-toxicity across 11 analyses, while Daidzein's reactivity surfaces in 5 out of 11 scenarios. Consistent with these observations, the Tox21 pathway corroborates L-arginine's non-toxicity compared to Daidzein. Furthermore, L-arginine establishes its eco-friendliness, manifesting lesser environmental toxicity when juxtaposed with Daidzein. An adjudication, facilitated by SwissADME (Fig. 10A and C) and ADMETLab 2.0 (Fig. 10B and D), collectively reverberates the therapeutic promise of L-arginine as an excellent drug candidate relative to Daidzein.

Ligands	Poses	Energy
CYP1A2		
Daidzein - O=C1C(c2ccc(O)cc2)=COc2c1ccc(O)c2	1	– 6.78727
	2	– 6.71767
	3	– 6.35044
	4	– 6.29579
	5	– 6.29216
L-arginine - O=C(O)[C@@H](N)CCC/N=C(\N)/N	1	– 5.68231
	2	– 5.51145
	3	– 5.42317
	4	– 5.41298
	5	– 5.32958
Metformin - N(\C(N(C)C)=N)=C(\N)/N	1	– 5.31141
	2	– 5.24249
	3	– 5.17449
	4	– 5.17066
	5	– 5.09862
CYP2C19		
Metformin - N(\C(N(C)C)=N)=C(\N)/N	1	– 5.08931
	2	– 4.88484
	3	– 4.88281
	4	– 4.78904
	5	– 4.58654
L-arginine - O=C(O)[C@@H](N)CCC/N=C(\N)/N	1	– 5.7561
	2	– 5.56947
	3	– 5.39879
	4	– 5.18215
	5	– 5.15937
Daidzein - O=C1C(c2ccc(O)cc2)=COc2c1ccc(O)c2	1	– 6.55574
	2	– 6.51544
	3	– 6.38638
	4	– 6.36012
	5	– 6.21629
NFKB-1		
Metformin - N(\C(N(C)C)=N)=C(\N)/N	1	– 4.50871
	2	– 3.22173
	3	– 3.07811
	4	– 3.01871
	5	– 2.90027
L-arginine - O=C(O)[C@@H](N)CCC/N=C(\N)/N	1	– 4.97617
	2	– 4.69486
	3	– 4.57247
	4	– 4.28701
	5	– 4.24928
Daidzein - O=C1C(c2ccc(O)cc2)=COc2c1ccc(O)c2	1	4.738304
	2	6.864085
	3	7.248343
	4	8.795058
	5	9.027375

Table 2. Molecular docking energy scores (indicated as S) of target compounds with the three common proteins.

Seed extract and oil preparation

The solution obtained from the filtration and sonication of fenugreek seeds exhibited a distinctive light yellow to golden hue (Fig. 11A), providing a visual confirmation of its origin from the seeds of the fenugreek plant. The seed oil extracted from fenugreek using the Soxhlet extraction method manifested a coloration ranging from dark yellow to a subdued golden color, as shown in Fig. 11B.
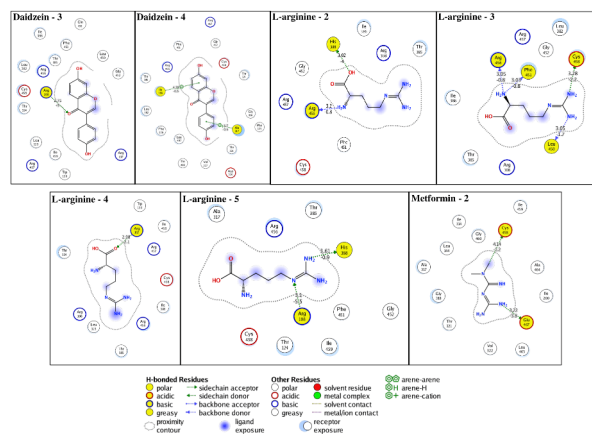
Fig. 7. 2D interaction profiles of different poses of L-arginine, Daidzein, and Metformin (Control) with CYP1A2 protein. The ligands are present in the center whereas the protein's surrounding amino acids are present around them. The amino acids shown in yellow are involved in direct molecular interaction with the ligands. The numbers represent the docking pose for each interaction.
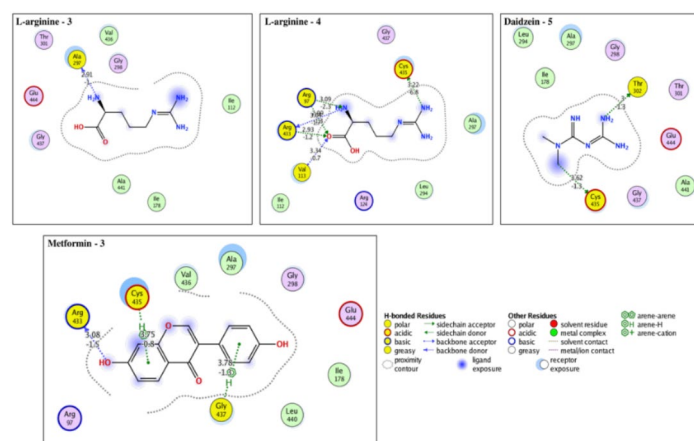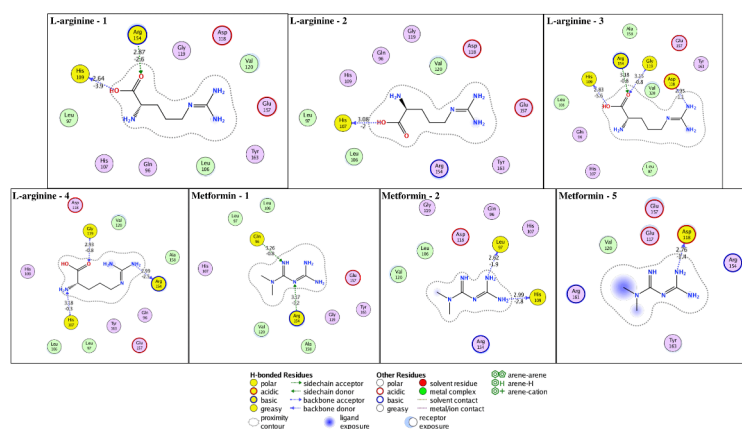

Fig. 8. 2D interaction profiles of different poses of L-arginine, Daidzein, and Metformin (Control) with CYP2C19 protein.

Fig. 9. 2D interaction profiles of different poses of L-arginine, Daidzein, and Metformin (Control) with NFKB1 protein.
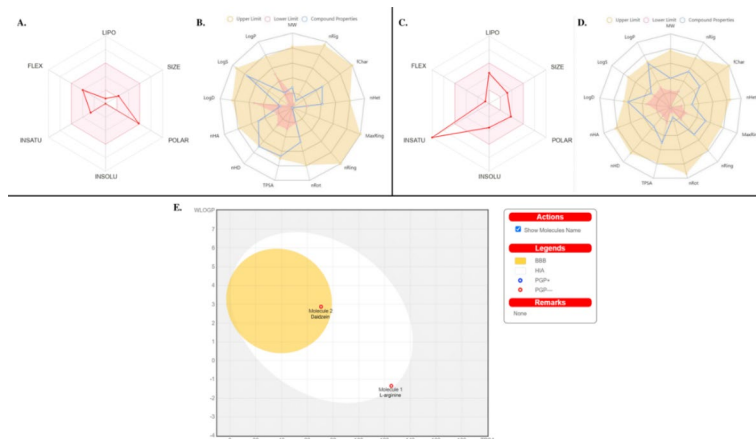
Fig. 10. ADMET profiles of the target compounds. A-B. ADMET profiles of L-arginine provided by SwissADME (A) and ADMETLab 2.0 (B); C-D. ADMET profiles of Daidzein provided by SwissADME (C) and ADMETLab 2.0 (D); E. The BOILED-Egg analysis of both compounds.
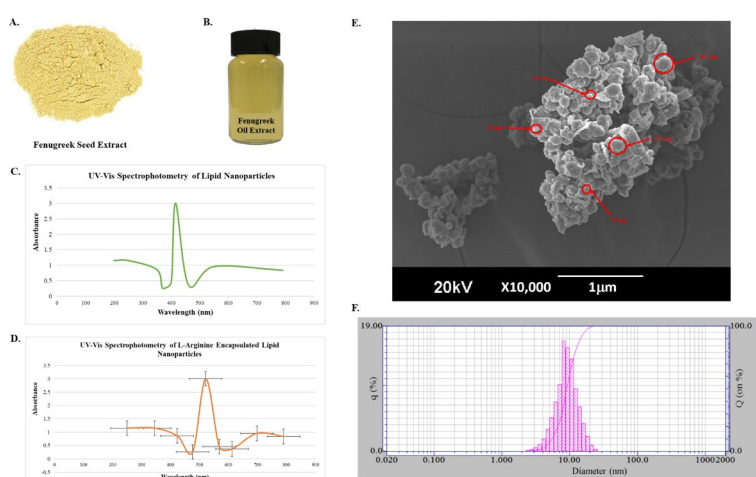

Fig. 11. Processing of fenugreek; (A) Seed extract; (B) Oil Extract; (C) UV-visible spectroscopy for synthesized lipid nanoparticles showing maximum peak at 415 nm using oil extract of fenugreek seeds as precursor with methanolic seed extract at 1:1; (D) UV visible spectroscopy for synthesized L-arginine encapsulated lipid nanoparticles showing maximum absorbance at 521 nm; (E) SEM micrograph of L-arginine encapsulated lipid nanoparticles synthesized by using seed and oil extract of fenugreek showing an average size of 100.2 nm at 10,000X and 1 micrometer known distance; (F) Size calculation of L-arginine-encapsulated lipid nanoparticles using PSD.

Phytochemical screening

Wagner's reagent revealed the presence of alkaloids in both fenugreek seeds and oil extract. It was substantiated by the formation of a distinct reddish-brown coloration upon reaction. The foam test implementation emphasized saponins' existence in both fenugreek seeds and the extracted oil. The generation of a persistent foam substantiated this observation upon rigorous agitation and gentle heating of the seed and oil extracts with distilled water. Other phytochemical screening analyses are discussed in Table 3.

Evaluation of total flavonoid content

The calculated concentrations were 285 mg/g (seed extract) and 225 mg/g (oil extract) in a solvent volume of 100 ml. Both extracts shared an equivalent dry weight of 20 g. The comparatively higher flavonoid concentration in the fenugreek seed extract (285 mg/g) than the oil extract (225 mg/g) implies that the seeds could serve as a richer source of these valuable phytochemicals.

Evaluation of total phenolic content

The determined phenolic content within the extracts derived from fenugreek seeds and oil yielded 335 mg/g and 195 mg/g, respectively, in a solvent volume of 100 ml. The substantial difference in phenolic content between

Sr #.	Screening test	Screened phytochemical	Inference	Result Extract	Oil
1.	Wagner's Test	Alkaloids	Appearance of reddish brown color with Wagner's reagent	+++	+++
2.	Foam Test	Saponins	Formation of stable foam	+++	+++
3.	Ferric Chloride Test	Phenols	Indication of blue green color with ferric chloride	+++	+++
4.	Braymer's Test	Tannins	Formation of green precipitates	---	---
5.	Salkowski's Test	Terpenoids	Appearance of yellow color	---	---
6.	Bontrager's Test	Quinones	Occurrence of red color in alkaline phase	+++	+++
7.	Keller Killani's Test	Cardiac Glycosides	Formation of pink to blood red coloration	---	---
8.	Glycosides Test	Glycosides	Indication of pink color	+++	+++
9.	Alkaline Reagent Test	Flavonoids	Formation of yellow color which becomes colorless on addition of acid	+++	+++
10.	Precipitate Test	Phlobatannins	Appearance of red precipitates	---	---

Table 3. Phytochemical screening of seed and oil extracts in fenugreek.

the fenugreek seed extract (335 mg/g) and the oil extract (195 mg/g) underscores the differential distribution of these bioactive compounds within the various parts of the fenugreek plant.

Synthesis of lipid nanoparticles

No palpable color alteration was noted throughout the lipid nanoparticle synthesis process. Nevertheless, using a UV-VIS spectrophotometer, the successful synthesis of lipid nanoparticles was validated using surface plasmon resonance analysis, at a wavelength of 415 nm (Fig. 11C). The absorbance peak at 415 nm corresponds to the characteristic SPR of lipid nanoparticles, which is indicative of their uniform size distribution and stability in suspension. This peak arises from the collective oscillation of surface electrons in response to light, a key feature confirming the formation of nanoparticles with consistent structural integrity.

Encapsulation of L-arginine in lipid nanoparticles

Upon the introduction of L-arginine to the lipid nanoparticle formulation, a subtle alteration in coloration was perceptible, transitioning from a golden yellow color to a lime yellow shade. However, after desiccation, the L-arginine encapsulated lipid nanoparticles exhibited a light greenish tint.

Characterization of encapsulated nanoparticles

The UV-Vis spectroscopic analysis revealed a prominent light absorbance peak for the L-arginine encapsulated lipid nanoparticles at a specific wavelength of 521 nm (Fig. 11D). This secondary peak at 521 nm is attributed to the successful encapsulation of L-arginine within the lipid matrix, as it reflects changes in the optical properties of the lipid nanoparticles due to the interaction between L-arginine molecules and the lipid carrier. The shift in absorbance compared to blank nanoparticles is a strong indicator of efficient loading and stabilization of L-arginine within the nanocarrier system. An illustrative scanning electron micrograph depicted the nanoparticles possessing a spherical configuration. Moreover, employing image analysis software, Image J, the average particle size was quantified at approximately 100.2 nm (Fig. 11E). The particle size is particularly suitable for cellular uptake in diabetes-related tissues, as particles within the range of 50–150 nm are known to enhance penetration through capillaries and provide efficient cellular internalization in targeted tissues.

The FTIR spectra revealed a spectrum of functional groups on the nanoparticle surface, contributing to its reduction and overall stability. An evident peak at 1007.72 cm^{-1} highlighted the presence of symmetrical and asymmetrical C–O vibrational stretching, affirming the participation of these bonds in the nanoparticle's constitution (Fig. 12A). In addition, the FTIR analysis exhibited a peak at 1636.46 cm^{-1}, indicative of C = C bonds present in the sample. The FTIR chart was read according to the reference tables provided by Sigma-Aldrich, available at: https://www.sigmaaldrich.com/PK/en/technical-documents/technical-article/analytical-chemistry/photometry-and-reflectometry/ir-spectrum-table. The results of the size distribution analysis indicated that the average size of the synthesized L-arginine-encapsulated lipid nanoparticles (NPs) is approximately 100 nm (Fig. 11E). This hydrodynamic size encompasses the hydration layer on the NP surface, leading to a measurement typically larger than the dimensions obtained from scanning electron microscopy (SEM) images. This size aligns well with the requirements for effective delivery to diabetes-related tissues, emphasizing its potential clinical relevance.

The obtained ζ-potential value was recorded as – 9.37 mV at a pH of 8.5, (Fig. 12B). While this neutral ζ-potential may reduce aggregation tendencies in biological systems, it also raises concerns regarding the stability of the nanoparticles, as strongly charged particles (zeta potentials exceeding + 30 mV or falling below – 30 mV) are generally more stable in suspension. This limitation highlights the need for further optimization or the incorporation of stabilizing agents to enhance colloidal stability. The X-ray Diffraction (XRD) analysis (Fig. 12C) revealed distinctive humped peaks indicative of short-range ordering within the nanoparticles. A subset of well-defined sharp peaks, notably at 44° (2theta), was also clear. This observation indicates the predominant amorphous character of the nanoparticles, with a subtle semblance of semi-crystalline attributes.
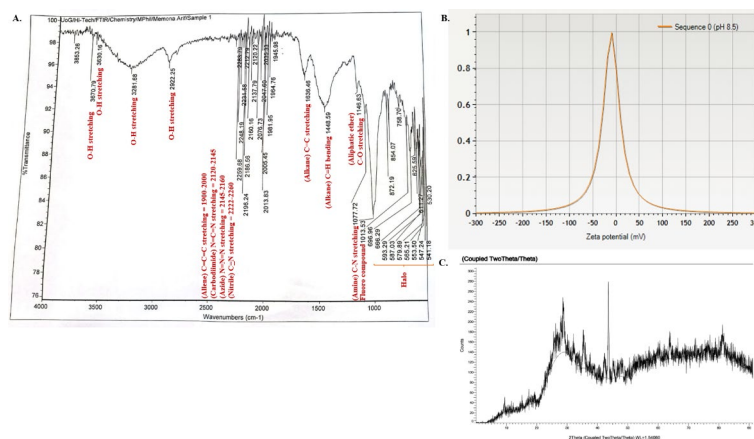
Fig. 12. Characterization of the nanoparticles. A. FTIR analysis of L-arginine encapsulated lipid nanoparticles; The calculated ζ-potential of the L-arginine-encapsulated lipid nanoparticles; XRD graph of L-arginine-encapsulated lipid nanoparticles indicating their amorphous to semi-crystalline nature.
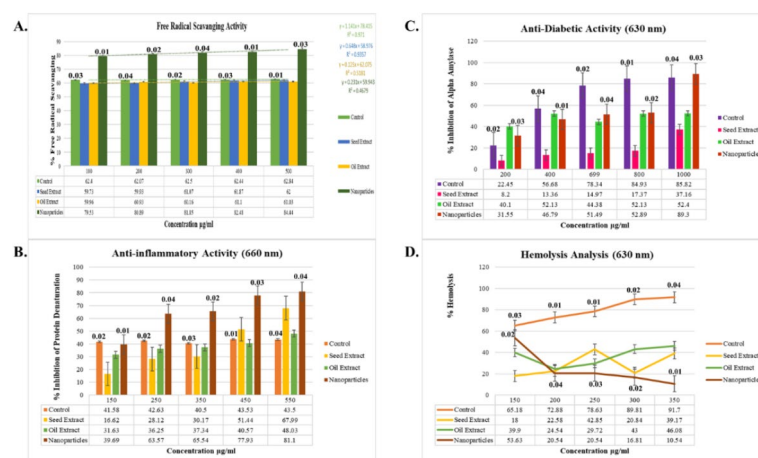

Fig. 13. Activities of the control, seed extract, oil extract, and L-arginine-encapsulated lipid nanoparticles at various concentrations; (A) Percentage of free radical scavenging; (B) Percentage inhibition of albumin denaturation; (C) anti-diabetic effect demonstrates the percentage inhibition of the α-amylase assay; (D) Hemolysis effect showing RBCs destruction. The one-way ANOVA indicates that all values are significant ($p < 0.05$) of nanoparticles compared to control.

Anti-oxidant activity

The lipid nanoparticles encapsulating L-arginine displayed significant antioxidant potential at the 500 μg/mL maximal concentration (Fig. 13A). Their antioxidative efficacy attained a remarkable magnitude of 84.44% and an IC50 value of 40.5. Statistical analysis ($p < 0.05$) confirmed that the antioxidative performance of the L-arginine encapsulated nanoparticles was significantly superior to the control (62.84%: IC50-231.27), fenugreek seed extract (59.73%: IC50-208.98), and oil extract (61.03%: IC50-196.6). It highlighted the nanoparticles' proficiency in radical scavenging, a quality potentially attributed to their specific composition and the presence of L-arginine.

Anti-inflammatory potential

The investigation evaluated the proficiency of L-arginine encapsulated lipid nanoparticles in inhibiting albumin denaturation over varying concentrations (Fig. 13B). Notably, amidst these concentrations, a concentration of 550 μg/mL exhibited an impressive 81.10% inhibition of albumin denaturation. This result was statistically higher ($p < 0.05$) than the control group (43.50%), seed extract (51.44%), and seed oil (31.63%), highlighting the enhanced anti-inflammatory potential conferred by L-arginine encapsulation.

Anti-diabetic activity

The observed inhibitory effect of the L-arginine encapsulated lipid nanoparticles exhibited a direct correlation with concentration (spanning from 200 μg/mL to 1000 μg/mL), demonstrating a dose-dependent relationship

(Fig. 13C). The alpha-amylase inhibition attributed to the L-arginine encapsulated lipid nanoparticles reached 89.30%, significantly surpassing ($p < 0.05$) the inhibition observed with metformin, a widely utilized antidiabetic medication, which exhibited a maximum inhibition of 78.43% at an equivalent dose (1000 µg/mL).

Hemolytic activity

The hemolysis percentage of 10.54% was recorded at the highest concentration of 350 µg/mL for the L-arginine encapsulated lipid nanoparticles (Fig. 13D). This value was statistically lower ($p < 0.05$) compared to the hemolysis percentages observed for the control (91.70%), fenugreek seed extract (39.17%), and fenugreek oil extract (46.08%). These results suggest excellent biocompatibility of the nanoparticles, making them suitable for biomedical applications.

Discussion

The widespread prevalence and nature of diabetes demand continuous research efforts to advance effective therapeutic strategies for improved patient outcomes[38]. This investigation explored the potential roles of L-arginine and fenugreek in diabetes management while also evaluating the efficacy of lipid nanocarriers for drug delivery in diabetes treatment. The findings provide a robust foundation for exploring the translational potential of L-arginine-encapsulated lipid nanoparticles as a promising anti-diabetic strategy.

Our results demonstrated the superior antioxidative, anti-inflammatory, and antidiabetic efficacy of L-arginine-encapsulated lipid nanoparticles compared to traditional treatments. This enhanced efficacy may be attributed to the nanoparticles' ability to improve bioavailability, protect L-arginine from premature degradation, and facilitate targeted delivery to cellular sites of action. The hydrogen bonding interactions observed during molecular docking (Figs. 8, 9 and 10) likely underpin the nanoparticles' strong binding affinity to key molecular targets, contributing to their remarkable therapeutic performance. This mechanism aligns with the established role of hydrogen bonds in mediating molecular interactions and enhancing drug-target specificity[39].

Our findings align with other studies in the field. For instance, in a study exploring antidiabetic peptides derived from hypoglycemic polypeptide-P of *M. charantia*[40], top-performing peptides were shortlisted based on S-scores and binding affinities. Similarly, a study on drug repurposing for α-glucosidase inhibition used FDA-approved drugs and identified promising molecular mechanisms[41]. Our study focused specifically on fenugreek seeds due to their prominence in various therapeutic applications. Both the leaves and seeds of fenugreek have been widely utilized in extracts and powders for therapeutic purposes, supported by numerous animal and human trials that have highlighted their hypoglycemic, hypolipidemic, and hypocholesterolemic effects[42,43]. This approach aligns with the findings of preliminary investigations, further substantiating the potential of fenugreek seeds as a valuable resource for therapeutic applications.

The determination of Total Flavonoid Content (TFC) within our fenugreek extracts imply that fenugreek seeds are a richer source of these valuable phytochemicals. Our results resonate with previous studies by Akbari et al.[44] and Al-Timimi[45], emphasizing the essential role of fenugreek seeds in addressing inflammation, cancer, and diabetes. Similarly, our Total Phenolic Content (TPC) findings parallel these observations. This consistency with prior research highlights a well-established trend where seed extracts exhibit higher TPC and TFC levels than oil extracts.

This difference in content can be attributed to various factors. The extraction process for seed extracts involves solvents like methanol or ethanol, which possess high solubility for phenolic compounds and flavonoids. It allows for effectively extracting and preserving a larger quantity of these compounds from the seeds, contributing to higher TPC and TFC levels[46]. Concentration processes used for seed extracts, such as evaporation or freeze-drying, further enhance phenolic and flavonoid content while reducing the extract volume[47]. Additionally, the broader range of compounds found in seed extracts, including phenolics and flavonoids, compared to the lipid-rich composition of seed oil extracts, explains the observed higher TPC and TFC levels in seed extracts[48].

The UV-Vis spectroscopic analysis identified distinct light absorbance peaks for the simple lipid nanoparticles at 415 nm and the L-arginine encapsulated lipid nanoparticles at 521 nm. Interestingly, no existing literature could be found either supporting or negating these specific peaks, stressing the novelty of our approach in synthesizing L-arginine encapsulated lipid nanoparticles. This unique spectral signature prompts further investigation into the underlying mechanisms governing these absorbance peaks. Our scanning electron microscopy (SEM) results align well with the size range reported by Rawat et al.[49]. Comparable studies by Parvez et al.[50] illustrated solid lipid nanoparticles encapsulated with Amphotericin B and Paromomycin, exhibiting a size of 140.2 ± 10.15 nm. Further literature[51] suggests that nanoparticles falling within the size range of 10 to 60 nm, irrespective of their surface charge or composition, are generally conducive to cellular uptake.

Moreover, nanoparticles below 200 nm exhibit enhanced passive transport into red blood cells (RBCs)[52]. Importantly, nanoparticles approximately 100 nm in size have demonstrated more than a threefold increase in arterial uptake compared to larger counterparts[53]. However, the interplay of composition, surface charge, and target cells or tissues can influence nanoparticle behavior and efficacy. Therefore, a comprehensive evaluation of nanoparticles in the context of specific applications and requirements is recommended. The neutral zeta potential of the synthesized nanoparticles presents challenges related to stability and aggregation. To overcome these issues, functionalizing nanoparticles with targeting ligands such as polyethylene glycol (PEG), aptamers, or antibodies could enhance stability and specificity. Alternatively, introducing surface coatings like chitosan or poloxamers can optimize interactions with biological components and improve drug delivery efficiency[54]. These strategies should form a key focus of any subsequent research.

Conversely, neutral zeta potential values may lead to reduced stability and heightened aggregation susceptibility[54], as seen in our SEM micrograph. Surface modification strategies, such as targeting ligands or using protective coatings, are often employed to enhance nanoparticle stability and optimize drug delivery[54].

Therefore, our near-future plans include surface modifications to augment zeta potential and enhance the stability and suitability of our nanoparticles for drug delivery applications.

The exploration of amorphous nanoparticles in the context of pharmaceuticals is an area yet to be extensively explored. Still, it is widely recognized that amorphous pharmaceutical formulations offer distinct advantages over their crystalline counterparts, particularly in dissolution and subsequent bioavailability properties[55]. Significantly, the amorphous structure promotes increased surface area and reduced diffusion distances, enabling more efficient dissolution in biological fluids[56]. This improvement in oral absorption can play a pivotal role in enhancing the therapeutic efficacy of such drugs.

While our study highlights the potential of L-arginine-based nanoparticles, the absence of in vivo validation remains a limitation. Future studies should involve animal models to validate these findings and assess pharmacokinetics, biodistribution, and long-term safety. Additionally, clinical trials will be essential to evaluate efficacy and tolerability in human subjects. The synthesis and application of nanoparticles raise significant environmental and ethical concerns. Our study incorporated green chemistry principles by adopting eco-friendly solvents and minimizing waste during nanoparticle synthesis, aiming to reduce the environmental footprint.

Although this is a step towards sustainable practices, the potential systemic effects and long-term toxicity of nanoparticles composed of different excipients warrant further exploration. Nanoparticles, depending on their composition, may exhibit varying degrees of biocompatibility or adverse systemic effects, including inflammation, oxidative stress, and cytotoxicity[57]. For instance, lipid-based nanoparticles, are generally considered biocompatible. The unique properties of lipids, such as biodegradability and biocompatibility, add to drug bioavailability through their specialized transport pathways. Hence, lipid-based particles improve gastrointestinal absorption and solubilization of poorly bioavailable drugs by facilitating selective lymphatic transport. Still, they may trigger immune responses or accumulate in the liver and spleen, leading to potential organ toxicity[59]. Studies[60,61] have reported that cationic lipid nanoparticles can be cytotoxic due to their interaction with cell membranes. However, neutral or anionic formulations, such as those used in our study, have demonstrated relatively safer profiles.

To address these concerns, future studies should evaluate the safety profiles of L-arginine encapsulated lipid nanoparticles through comprehensive in vitro and in vivo toxicological assessments. Such evaluations should include biodistribution studies to understand the fate of nanoparticles within biological systems and their potential accumulation in vital organs. Additionally, the environmental impact of nanoparticle disposal and their potential bioaccumulation in ecosystems should be assessed. Ethical considerations, including the humane treatment of animals during in vivo studies, should remain a priority, adhering to established guidelines. These efforts are important to ensure that nanoparticles designed for therapeutic applications maintain a balance between efficacy and safety while minimizing their ecological and systemic impact.

Comparison of this work with literature

The results of our study align well with existing research in several areas. Our molecular docking analysis using MOE software, emphasizing S scores, is consistent with similar approaches in studies on antidiabetic peptides[40] and drug repurposing for α-glucosidase inhibition[41]. The therapeutic potential of fenugreek seeds, highlighted by their higher total flavonoid and phenolic content compared to oil extracts, aligns with findings from Akbari et al.[44] and Al-Timimi[45], as well as the therapeutic benefits reported by Visuvanathan et al.[42] and Wani & Kumar[43]. Our nanoparticle size of approximately 100 nm is within the effective range for cellular uptake, as supported by studies from Rawat et al.[49], Parvez et al.[50], and Sabourian et al.[51]. The need for surface modifications to improve zeta potential and stability is consistent with Clogston & Patri[62] and Honary & Zahir[54]. Additionally, the amorphous nature of our nanoparticles, offering enhanced dissolution and bioavailability, aligns with the benefits outlined by Valenti et al.[55] and Andrews et al.[56]. Lastly, our antioxidative efficacy and lower hemolysis percentage compared to controls highlight the therapeutic potential of our nanoparticles, as seen in other research findings. Unlike earlier studies focusing on broad-spectrum applications, this research directly targets diabetes, showcasing the innovative potential of combining fenugreek bioactive metabolites with nanotechnology. The distinct UV-Vis absorbance peaks observed for our nanoparticles at 521 nm further highlight the novelty of our synthesis approach. These findings surpass previous efforts by presenting a more effective and targeted therapeutic intervention.

Conclusion

The study's findings advocate the promising potential of L-arginine, especially when encapsulated within lipid nanoparticles, as an effective anti-diabetic agent. The molecular interactions of L-arginine with key diabetes-target genes (CYP1A2, CYP2C19, and NFKB) reinforce its therapeutic promise. The strategic focus on Fenugreek's bioactive compounds provided a solid foundation for identifying L-arginine as a lead compound. The UV-Vis spectroscopic and scanning electron microscopy analyses confirmed the successful synthesis of L-arginine encapsulated lipid nanoparticles, with novel spectral signatures and optimal nanoparticle sizes conducive to cellular uptake. The neutral zeta potential of the nanoparticles, while initially posing a stability challenge, opens avenues for future surface modification strategies to enhance stability and drug delivery efficiency. The amorphous nature of these nanoparticles, confirmed by X-ray diffraction, points to significant advantages in drug dissolution and bioavailability, potentially revolutionizing oral absorption strategies for poorly water-soluble drugs. Most notably, the antioxidative efficacy of L-arginine encapsulated lipid nanoparticles, surpassing other tested extracts and controls, highlights their superior therapeutic potential. To translate these findings into clinical practice, future efforts should focus on scaling up the production process to ensure consistency and cost-effectiveness. Establishing protocols for large-scale synthesis while maintaining the nanoparticles' physicochemical properties will be critical for commercial viability. Additionally, tailored formulations targeting

specific patient populations, such as those with Type 2 diabetes or coexisting cardiovascular complications, could maximize therapeutic benefits and minimize side effects. Our study, despite having thorough laboratory evidence, has several limitations, including the lack of in vivo validation, absence of surface modification for nanoparticle stability, and detailed size distribution analysis. Additionally, long-term stability and potential side effects were not assessed. We also did not compare simple lipid nanoparticles with encapsulated ones. Future work should address these limitations, explore scalability, reproducibility, regulatory requirements for clinical applications, environmental impact, evaluate patient-specific efficacy, and provide deeper mechanistic insights to improve the therapeutic potential of L-arginine encapsulated lipid nanoparticles and other such delivery methods. This study, nonetheless, paves the way for developing other innovative therapeutic strategies utilizing the unique properties of encapsulated lipid nanoparticles. These findings contribute to the broader scientific discourse on diabetes management, offering a novel and promising avenue for improving patient outcomes.

Data availability
All data supporting the findings of this study are available within the paper.

References
1. Wei, Y. et al. Exploring the causal relationships between type 2 diabetes and neurological disorders using a Mendelian randomization strategy. *Medicine* **103**, e40412 (2024).
2. International Diabetes Federation. *Diabetes around the World in 2021* (IDF Diabetes Atlas, 2022).
3. Hossain, J., Al-Mamun, M. & Islam, M. R. Diabetes mellitus, the fastest growing global public health concern: early detection should be focused. *Health Sci. Rep.* **7** (2024).
4. Cheng, X. et al. Quercetin: A promising therapy for diabetic encephalopathy through Inhibition of hippocampal ferroptosis. *Phytomedicine* **126**, 154887 (2023).
5. Liang, J. et al. The regulation of selenoproteins in diabetes: A new way to treat diabetes. *Curr. Pharm. Des.* **30**, 1541–1547 (2024).
6. Rahman, M. M. et al. Exploring the plant-derived bioactive substances as antidiabetic agent: an extensive review. *Biomed. Pharmacother.* **152**, 113217–113217 (2022).
7. Dai, B. et al. The effect of Liuwei Dihuang Decoction on PI3K/Akt signaling pathway in liver of type 2 diabetes mellitus (T2DM) rats with insulin resistance. *J. Ethnopharmacol.* **192**, 382–389 (2016).
8. Singh, N., Yadav, S. S., Kumar, S. & Narashiman, B. Ethnopharmacological, phytochemical and clinical studies on Fenugreek (*Trigonella foenum-graecum* L.). *Food Biosci.* **46**, 101546 (2022).
9. Dirir, A. M., Daou, M., Yousef, A. F. & Yousef, L. F. A review of alpha-glucosidase inhibitors from plants as potential candidates for the treatment of type-2 diabetes. *Phytochem Rev.* (2021).
10. Hosseini, S. A., Hamzavi, K., Safarzadeh, H. & Salehi, O. Interactive effect of swimming training and Fenugreek (*Trigonella foenum graecum L.*) extract on glycemic indices and lipid profile in diabetic rats. *Arch. Physiol.* 1–5 (2020).
11. Haxhiraj, M., White, K. & Terry, C. The role of Fenugreek in the management of type 2 diabetes. *Int. J. Mol. Sci.* **25**, 6987 (2024).
12. Carvalho, D. S. et al. L-Arginine supplementation improves insulin sensitivity and beta cell function in the offspring of diabetic rats through AKT and PDX-1 activation. *Eur. J. Pharm.* **791**, 780–787 (2016).
13. Losada-Barragán, M. Physiological effects of nutrients on insulin release by pancreatic beta cells. *Mol. Cell. Biochem.* **476**, 3127–3139 (2021).
14. Forzano, I. et al. L-Arginine in diabetes: clinical and preclinical evidence. *Cardiovasc. Diabetol.* 22 (2023).
15. Chen, Y. M. et al. Supplementation of L-Arginine, L-Glutamine, Folic Acid, and Green Tea Extract Enhances Serum Nitric Oxide Content and Antifatigue Activity in Mice. *eCAM.* 1–10 (2020). (2020).
16. Farkhani, S. M. et al. Cell penetrating peptides: efficient vectors for delivery of nanoparticles, nanocarriers, therapeutic and diagnostic molecules. *Peptides* **57**, 78–94 (2014).
17. Böttger, R. et al. Lipid-based nanoparticle technologies for liver targeting. *Adv. Drug Deliv Rev.* **154–155**, 79–101 (2020).
18. Tariq, A. et al. Herbal medicines used to treat diabetes in Southern regions of Pakistan and their Pharmacological evidence. *J. Herb. Med.* **21**, 100323 (2020).
19. Kiss, R. et al. Insulin-Sensitizer effects of Fenugreek seeds in parallel with changes in plasma MCH levels in healthy volunteers. *Int. J. Mol. Sci.* **19**, 771 (2018).
20. Srinivasa, U. M. & Naidu, M. M. Chapter 6 - Fenugreek (*Trigonella foenum-graecum* L.) seed: promising source of nutraceutical. *ScienceDirect* **71**, 141–184 (2021).
21. Zheng, J. et al. A polyphenolic curcuminoid with its protective effects and molecular mechanisms in diabetes and diabetic cardiomyopathy. *Front. Pharmacol.* **9** (2018).
22. Bateman, A. et al. UniProt: the universal protein knowledgebase in 2023. *Nucleic Acids Res.* **51** (2022).
23. Stelzer, G. et al. The genecards suite: from gene data mining to disease genome sequence analyses. *Curr. Protoc. Bioinform.* **54**, 1301–13033 (2016).
24. Oliveros, J. C. Venny. An interactive tool for comparing lists with Venn's diagrams (2015).
25. Shannon, P. & Cytoscape A software environment for integrated models of biomolecular interaction networks. *Genome Res.* **13**, 2498–2504 (2003).
26. Szklarczyk, D. et al. The STRING database in 2023: protein–protein association networks and functional enrichment analyses for any sequenced genome of interest. *Nucleic Acids Res.* **51**, D638–D646 (2022).
27. Vilar, S., Cozza, G. & Moro, S. Medicinal chemistry and the molecular operating environment (MOE): application of QSAR and molecular Docking to drug discovery. *Curr. Top. Med. Chem.* **8**, 1555–1572 (2008).
28. Berman, H. M. The protein data bank. *Nucleic Acids Res.* **28**, 235–242 (2000).
29. Xu, X. et al. A novel chemometric method for the prediction of human oral bioavailability. *Int. J. Mol. Sci.* **13**, 6964–6982 (2012).
30. Daina, A., Michielin, O. & Zoete, V. SwissADME: a free web tool to evaluate pharmacokinetics, drug-likeness and medicinal chemistry friendliness of small molecules. *Sci. Rep.* 7 (2017).
31. Xiong, G. et al. ADMETlab 2.0: an integrated online platform for accurate and comprehensive predictions of ADMET properties. *Nucleic Acids Res.* **49**, W5–W14 (2021).
32. Singleton, V. L., Orthofer, R. & Lamuela-Raventós, R. M. Analysis of total phenols and other oxidation substrates and antioxidants by means of folin-ciocalteu reagent. *ScienceDirect* **299**, 152–178 (1999).
33. Naveed, M. et al. Biosynthesis and mathematical interpretation of Zero-Valent Iron NPs using Nigella sativa seed tincture for indemnification of carcinogenic metals present in industrial effluents. *Molecules* **28**, 3299 (2023).
34. Ghosh, P. et al. Nanoencapsulation as a promising platform for the delivery of the Morin-Cu(II) complex: antibacterial and anticancer potential. *ACS Omega.* **7**, 7931–7944 (2022).

35. Ghosh, P. et al. Solubility enhancement of Morin and epicatechin through encapsulation in an albumin based nanoparticulate system and their anticancer activity against the MDA-MB-468 breast cancer cell line. *RSC Adv.* **6**, 101415–101429 (2016).
36. Bera, A., Ghosh, P., Ghosh, S., Mukherjee, A. & De, P. Antioxidant polymers with enhanced neuroprotection against insulin fibrillation. *Macromol. Biosci.* 23 (2023).
37. Bera, A., Ghosh, P., Goswami, K. & De, P. Amino Acid-Based Polymer-Coated silver nanoparticles as insulin fibril inhibitors. *ACS Appl. Nano Mater.* **6**, 8705–8716 (2023).
38. Tiwari, P. Recent Trends in Therapeutic Approaches for Diabetes Management: A Comprehensive Update. *J. Diabetes Res.* 1–11 (2015). (2015).
39. Chen, D. et al. Regulation of protein-ligand binding affinity by hydrogen bond pairing. *Sci. Adv.* **2** (2016).
40. Arif, R. et al. Molecular Docking and Simulation Studies of Antidiabetic Agents Devised from Hypoglycemic Polypeptide-P of Momordica charantia. *BioMed Res. Int.* e5561129 (2021). (2021).
41. Saeed, R. et al. Drug repurposing of FDA compounds against α-Glucosidase for the treatment of type 2 diabetes: insights from molecular Docking and molecular dynamics simulations. *Pharmaceuticals* **16**, 555–555 (2023).
42. Visuvanathan, T., Than, L. T. L., Stanslas, J., Chew, S. Y. & Vellasamy, S. Revisiting Trigonella foenum-graecum L.: Pharmacology and therapeutic potentialities. *Plants* **11**, 1450 (2022).
43. Wani, S. A., Kumar, P. & Fenugreek A review on its nutraceutical properties and utilization in various food products. *J. Saudi Soc. Agric. Sci.* **17**, 97–106 (2018).
44. Akbari, S., Abdurahman, N. H., Yunus, R. M., Alara, O. R. & Abayomi, O. O. Extraction, characterization and antioxidant activity of Fenugreek (*Trigonella-Foenum Graecum*) seed oil. *Mater. Sci. Energy Technol.* **2**, 349–355 (2019).
45. Al-Timimi, L. A. N. Antibacterial and anticancer activities of Fenugreek seed extract. *Asian Pac. J. Cancer P.* **20**, 3771–3776 (2019).
46. Phuyal, N., Jha, P. K., Raturi, P. P. & Rajbhandary, S. Total phenolic, flavonoid contents, and antioxidant activities of fruit, seed, and bark extracts of Zanthoxylum armatum DC. *Sci. World J.* (2020).
47. Zulkifli, S. A., Gani, A., Zaidan, S. S., Halmi, M. I. E. & U. H. & Optimization of total phenolic and flavonoid contents of defatted Pitaya (Hylocereus polyrhizus) seed extract and its antioxidant properties. *Molecules* **25**, 787 (2020).
48. Saeed, N., Khan, M. R. & Shabbir, M. Antioxidant activity, total phenolic and total flavonoid contents of whole plant extracts Torilis leptophylla L. *BMC Complement. Altern. Med.* **12** (2012).
49. Rawat, M. K., Jain, A. & Singh, S. Studies on binary lipid matrix based solid lipid nanoparticles of repaglinide: in vitro and *in vivo* evaluation. *J. Pharm. Sci.* **100**, 2366–2378 (2011).
50. Parvez, S. et al. Modified solid lipid nanoparticles encapsulated with amphotericin B and paromomycin: an effective oral combination against experimental murine visceral leishmaniasis. *Sci. Rep.* 10 (2020).
51. Sabourian, P. et al. Effect of Physico-Chemical properties of nanoparticles on their intracellular uptake. *Int. J. Mol. Sci.* **21**, 8019 (2020).
52. Hoshyar, N., Gray, S., Han, H. & Bao, G. The effect of nanoparticle size on *in vivo* pharmacokinetics and cellular interaction. *Nanomedicine* **11**, 673–692 (2016).
53. Prabha, S., Arya, G., Chandra, R., Ahmed, B. & Nimesh, S. Effect of size on biological properties of nanoparticles employed in gene delivery. *Artif. Cell. Nanomed. B.* **44**, 83–91 (2014).
54. Honary, S. & Zahir, F. Effect of zeta potential on the properties of Nano-Drug delivery Systems - A review (Part 2). *Trop. J. Pharm. Res.* **12** (2013).
55. Valenti, S. et al. Comparative physical study of three pharmaceutically active benzodiazepine derivatives: crystalline versus amorphous state and crystallization tendency. *Mol. Pharm.* 18 (2021).
56. Andrews, G. P., Qian, K., Jacobs, E., Jones, D. S. & Tian, Y. High drug loading nanosized amorphous solid dispersion (NASD) with enhanced in vitro solubility and permeability: benchmarking conventional ASD. *Int. J. Pharm.* **632**, 122551 (2023).
57. Kyriakides, T. R. et al. Biocompatibility of nanomaterials and their immunological properties. *Biomed. Mater.* 16 (2021).
58. Gangavarapu, A. et al. Lipid nanoparticles for enhancing oral bioavailability. *Nanoscale* 16 (2024).
59. Wang, J. et al. Recent advances in lipid nanoparticles and their safety concerns for mRNA delivery. *Vaccines* **12**, 1148 (2024).
60. Yuan, Z., Yan, R., Fu, Z., Wu, T. & Ren, C. Impact of physicochemical properties on biological effects of lipid nanoparticles: are they completely safe. *Sci. Total Environ.* **927**, 172240 (2024).
61. Hald Albertsen, C. et al. The role of lipid components in lipid nanoparticles for vaccines and gene therapy. *Adv. Drug Deliv. Rev.* 188, 114416 (2022). (2022).
62. Clogston, J. D. & Patri, A. K. Zeta potential measurement. *Methods Mol. Biol.* 63–70 (2010).

Author contributions

Conceptualization, Urooj Ali; methodology, Syeda Izma Makhdoom; software, Muhammad Uzair Javed; validation, Rafia Ali Khan; formal analysis, Muhammad Naveed, investigation, Urooj Ali; resources, Bilal Haider Abbasi.; data curation, Tariq Aziz.; writing—original draft preparation, Urooj Ali.; writing—review and editing, Fatma Alshehri, Fahad Al-Asmari, Fakhria A. Al-Joufi and Maher S. Alwethaynani; visualization, Muhammad Naveed; supervision, Bilal Haider Abbas and Tariq Aziz.; project administration, Bilal Haider Abbasi.

Funding

Competing interests

The authors declare no competing interests.

Ethical approval

This study doesn't involve any human or animal so ethical approval is not required for this study. This study was conducted under the local laws/legislation.

Additional information

Correspondence and requests for materials should be addressed to B.H.A. or T.A.